THE JOURNAL OF BIOLOGICAL CHEMISTRY VOL. 281, NO. 52, pp. 40473–40484, December 29, 2006

Molecular Architecture of the Glucose 1-Phosphate Site in ADP-glucose Pyrophosphorylases*[S]

Received for publication, July 25, 2006, and in revised form, November 1, 2006 Published, JBC Papers in Press, November 1, 2006, DOI 10.1074/jbc.M607088200

Clarisa Maria Bejar, Xiangshu Jin[1], Miguel Angel Ballicora[2], and Jack Preiss[3]

From the Department of Biochemistry and Molecular Biology, Michigan State University, East Lansing, Michigan 48824

ADP-Glc pyrophosphorylase (PPase), a key regulatory enzyme in the biosynthetic pathway of starch and bacterial glycogen, catalyzes the synthesis of ADP-Glc from Glc-1-P and ATP. A homology model of the three-dimensional structure of the *Escherichia coli* enzyme complexed with ADP-Glc has been generated to study the substrate-binding site in detail. A set of amino acids in the model has been identified to be in close proximity to the glucose moiety of the ADP-Glc ligand. The role of these amino acids (Glu^{194}, Ser^{212}, Tyr^{216}, Asp^{239}, Phe^{240}, Trp^{274}, and Asp^{276}) was studied by site-directed mutagenesis through the characterization of the kinetic properties and thermal stability of the designed mutants. All purified alanine mutants had 1 or 2 orders of magnitude lower apparent affinity for Glc-1-P compared with the wild type, indicating that the selected set of amino acids plays an important role in their interaction with the substrate. These amino acids, which are conserved within the ADP-Glc PPase family, were replaced with other residues to investigate the effect of size, hydrophobicity, polarity, aromaticity, or charge on the affinity for Glc-1-P. In this study, the architecture of the Glc-1-P-binding site is characterized. The model overlaps with the Glc-1-P site of other PPases such as *Pseudomonas aeruginosa* dTDP-Glc PPase and *Salmonella typhi* CDP-Glc PPase. Therefore, the data reported here may have implications for other members of the nucleotide-diphosphoglucose PPase family.

The biosynthetic pathways of starch and bacterial glycogen are very similar (1). The initial and key regulatory step is the formation of the glucosyl donor molecule ADP-Glc from ATP and Glc-1-P via a reaction catalyzed by ADP-glucose pyrophosphorylase (PPase[4]; glucose-1-phosphate adenylyltransferase, EC 2.7.7.27), with the requirement of a divalent cation (Mg^{2+}): ATP + Glc-1-P ← Mg^{2+} → ADP-Glc + PP_i.

Most ADP-Glc PPases are allosterically regulated by small effector molecules. Although these vary according to the source, they are all intermediates of the principal carbon assimilation pathway in the respective cell (2–6). Thus, bacterial glycogen and plant starch syntheses are not modulated only by the availability of ATP but also by the accumulation of key metabolites that represent the carbon and energy balance within the cell. For instance, the enzymes from heterotrophic bacteria such as *Escherichia coli* are regulated by intermediates of the glycolytic pathway, with Fru-1,6-P_2 as the main activator and AMP as the main inhibitor. On another hand, the ADP-Glc PPases from cells performing oxygenic photosynthesis and assimilating atmospheric CO_2 through the reductive pentose phosphate pathway or the Calvin cycle (specifically cyanobacteria, green algae, and photosynthetic tissues from higher plants) are activated by 3-phosphoglycerate and inhibited by P_i (6).

Except for some *Bacillus* species (5–7), prokaryotic ADP-Glc PPases are homotetramers, with the monomer being ~50 kDa (2, 5, 8, 9). Characterized ADP-Glc PPases from higher plants are heterotetramers of two different but homologous subunits (2–6), the "small" or catalytic subunit (50–54 kDa) and the "large" or regulatory subunit (51–60 kDa) (10). The small subunits are highly homologous (85–95% identity), whereas the large subunits have greater divergence (50–60% identity between them) and share ~50% identity with the small subunits (11, 12). Cyanobacterial ADP-Glc PPase shares features of both bacterial and plant enzymes. The native enzyme is a homotetramer, similar to the bacterial enzyme, but is regulated by 3-phosphoglycerate and P_i, like the plant enzyme, and is also immunologically more related to the plant enzyme (13).

The first ADP-Glc PPase crystal structure became recently available when Jin *et al.* (14) solved that of the homotetrameric *Solanum tuberosum* (potato tuber) small subunit in its allosterically inhibited form at a resolution of 2.1 Å. They also reported the structural determination of the enzyme complexed with either ATP or ADP-Glc at 2.6 and 2.2 Å, respectively. Attempts to obtain information on the *E. coli* enzyme structure through x-ray crystallography were unsuccessful. The potato tuber small subunit has only ~33% sequence identity to the *E. coli* enzyme, but the similar predicted secondary structure profile, together with available biochemical data, suggests that they share a common three-dimensional fold (5).

Previous chemical modification (15) and site-directed mutagenesis (16) studies on *E. coli* ADP-Glc PPase identified Lys^{195} as an important residue for Glc-1-P interaction. Replace-

* This work was supported by Research Grant IS-3733-05R from the United States-Israel Binational Agricultural Research and Development Fund and by Research Grant DE-FG02-93ER20121 from the Department of Energy. The costs of publication of this article were defrayed in part by the payment of page charges. This article must therefore be hereby marked "*advertisement*" in accordance with 18 U.S.C. Section 1734 solely to indicate this fact.

[S] The on-line version of this article (available at http://www.jbc.org) contains supplemental Fig. 1 and Table 1.

[1] Present address: Dept. of Biochemistry and Molecular Biophysics, Columbia University, New York, NY 02138.

[2] Present address: Dept. of Chemistry, Loyola University Chicago, Chicago, IL 60626.

[3] To whom correspondence should be addressed: Dept. of Biochemistry and Molecular Biology, 309 Biochemistry Bldg., Michigan State University, East Lansing, MI 48824. Tel.: 517-353-3437; Fax: 517-353-9334; E-mail: preiss@msu.edu.

[4] The abbreviation used is: PPase, pyrophosphorylase.

ment with other amino acids generated 100–10,000-fold increases in the $S_{0.5}$ for this substrate, with all other kinetic constants at wild-type levels. Later, Fu *et al.* (17) reported similar results from analysis of the homologous Lys^{198} in the potato tuber catalytic subunit. The proposed role of this amino acid is to form an ionic bond between the ϵ-amino group and the negatively charged phosphate of Glc-1-P. Results with Hex-1-P analogs, which differ from Glc-1-P in their hydroxyl groups, suggest that other residues in the active site participate in substrate binding.

Our aim was to obtain structural information on *E. coli* ADP-Glc PPase by building a homology model and to probe a set of highly conserved residues in the N-terminal domain possibly involved in Glc-1-P binding. We studied the role of Glu^{194}, Ser^{212}, Tyr^{216}, Asp^{239}, Phe^{240}, Trp^{274}, and Asp^{276} by site-directed mutagenesis and kinetic characterization of the mutant enzymes and their thermal stability. All residues were replaced with alanine and other amino acids to evaluate the importance of size, charge, or hydrophobicity on the effects observed in substrate interaction.

Because these residues are highly conserved among ADP-Glc PPases, it was of interest to investigate whether they are present in other PPases that use Glc-1-P as a substrate. The observations made by comparison of the putative Glc-1-P site from our *E. coli* ADP-Glc PPase model and the reported crystal structures of two pyrophosphorylases, the *Pseudomonas aeruginosa* dTDP-Glc PPase Rm1A (18) and *Salmonella typhi* CDP-Glc PPase (19), have led us to propose that the results presented here have implications beyond the family of ADP-Glc PPases.

EXPERIMENTAL PROCEDURES

Materials

Oligonucleotides were synthesized and purified at the Macromolecular Facility of Michigan State University. $[^{32}P]PP_i$ was purchased from PerkinElmer Life Sciences, and $[^{14}C]$Glc-1-P from ICN Pharmaceuticals, Inc. Sodium PP_i, ATP, ADP-Glc, AMP, and inorganic pyrophosphatase were purchased from Sigma. *Pfu* DNA polymerase was purchased from Stratagene (La Jolla, CA). All other reagents were of the highest quality available.

Homology Modeling

Comparative (homology) modeling of *E. coli* ADP-Glc PPase (residues 12–431) was carried out with MODELLER6 Version 1 (20–22) using the atomic coordinates of *S. tuberosum* ADP-Glc PPase small subunit chain B complexed with ADP-Glc (Protein Data Bank code 1YP2) (14) as a template. Sequence alignment was performed manually to match functionally conserved residues, predicted secondary structures, and hydrophobicity profiles. Secondary structures were predicted using the PredictProtein (www.predictprotein.org) and PSIPRED (bioinf.cs.ucl.ac.uk/psipred/) programs. The models were assessed by the VERIFY_3D program (nihserver.mbi.ucla.edu/Verify_3D/) (23, 24).

Multiple Sequence Alignment

A multiple sequence alignment was generated using the server ClustalW (www.ebi.ac.uk/clustalw) with representative ADP-Glc PPases belonging to different bacterial and plant taxa. The sequences used were from *E. coli* B (NCBI accession number P0A6V1) (25), *Agrobacterium tumefaciens* (P39669) (26), *Synechococcus* sp. WH 8102 (NP_897211) (27), *Thermotoga maritima* (Q9WY82) (28), *Streptococcus pneumoniae* (Q97QS7) (29), *Vibrio cholerae* (Q9KLP4) (30), *Clostridium cellulolyticum* (Q9L385), *Geobacillus stearothermophilus* (O08326) (7), *Mycobacterium tuberculosis* (O05314) (31), *Deinococcus radiodurans* (Q9RTR7) (32), *Anabaena* sp. PCC 7120 (P30521) (33), *Arabidopsis thaliana* (APS1 small subunit; P55228) (34), *S. tuberosum* (small subunit; P23509) (35), *Zea mays* (small subunit, endosperm; AAK69627) (36), and *Chlamydomonas reinhardtii* (small subunit; AAF75832) (37).

Site-directed Mutagenesis

Site-directed mutagenesis was performed by overlap extension PCR (38). Plasmid pMAB3 containing the *E. coli* ADP-Glc PPase gene between NdeI and SacI sites, previously obtained in our laboratory,[5] was used as a template. The flanking primers, which annealed with the T7 promoter and the SacI site (underlined) were 5′-TAATACGACTCACTATAGGG-3′ and 5′-GATATCTGAATTCGAGCTC-3′, respectively. The overlapping primers for each mutant are depicted in supplemental Table 1. The final PCR products were gel-purified, digested with NdeI and SacI, and subcloned to obtain the different pMAB3-single mutant plasmids. Plasmid pETEC-NΔ15-D276N was obtained using pETEC-NΔ15 (39) as a template, with the T7 promoter and T7 terminator as flanking primers and the same mutated overlapping primers used for pMAB3-D276N (supplemental Table 1). All plasmids were sequenced at the Genomics Facility of Michigan State University to confirm incorporation of only the desired mutation.

Bacterial Strains and Expression of Recombinant ADP-Glc PPases

E. coli AC70R1-504 cells lacking endogenous ADP-Glc PPase activity were used for expression of the wild-type and pMAB3-mutant enzymes as described previously for pML10 (35). EcNΔ15-D276N was expressed as EcNΔ15 (39).

Purification of pMAB3-Single Mutant Plasmids

One-liter cultures of AC70R1-504 cells transformed with the pMAB3-single mutant plasmids or BL21(DE3) cells transformed with pETEC-NΔ15-D276N were grown in 25 μg/ml kanamycin/Luria broth (1 liter) at 37 °C up to $A_{600} = 0.8$. Induction was initiated by the addition of isopropyl β-D-thiogalactopyranoside (1 mM final concentration), with subsequent incubation at 25 °C for 16 h. After induction, cells were harvested, and crude extracts were obtained as described previously (35). After centrifugation, the precipitate was resuspended in buffer A (50 mM Hepes (pH 8.0), 5 mM $MgCl_2$, 0.1 mM EDTA, and 10% sucrose). The samples were individually applied to a DEAE-Fractogel column (EMD Biosciences) and eluted with a linear gradient of 0–0.5 M NaCl. The active fractions were pooled and desalted. After this step, samples were 60–70% pure and suitable for performing kinetic analysis. Mutants E194A/Q/D,

[5] M. A. Ballicora and J. Preiss, unpublished data.

D276A/N, W274A, Y216F, and D239N were resuspended in buffer B (buffer A plus 1.2 M ammonium sulfate); applied to a phenyl-Superose fast protein liquid chromatography column (GE Healthcare) equilibrated with buffer B; and eluted with a linear gradient of 1.2 to 0.001 M ammonium sulfate. Further purification of the rest of the mutants and the wild type was performed by applying the DEAE pool samples to a Matrex™ gel green A affinity chromatography column (Amicon Corp.) and eluting with a linear gradient of 0–2 M NaCl. The purest fractions of each enzyme were pooled, desalted, and concentrated; and after these steps, the proteins were >95% pure as assessed by SDS-PAGE (data not shown).

Protein Methods

Protein assay, electrophoresis (SDS-PAGE), and immunoblotting were performed following protocols described previously (40). Samples were desalted and concentrated with Centricon-30 devices (Amicon Corp.).

Enzyme Assays

Assay A: Pyrophosphorolysis Direction—Formation of [^{32}P]ATP from [^{32}P]PP_i was determined by the method of Morell *et al.* (41). The reaction was carried out for 10 min at 37 °C in a mixture containing 50 mM Hepes (pH 8.0), 10 mM $MgCl_2$, 1.5 mM [^{32}P]PP_i (1500–2500 dpm/nmol), 4 mM ADP-Glc, 4 mM NaF, 2 mM Fru-1,6-P_2, and 0.05 mg/ml bovine serum albumin plus enzyme in a total volume of 0.25 ml.

Assay B: Synthesis Direction—Formation of ADP-[^{14}C]Glc from [^{14}C]Glc-1-P was determined by the method of Yep *et al.* (42). The reaction was carried out for 10 min at 37 °C in a mixture containing [^{14}C]Glc-1-P (~400 dpm/nmol), ATP, $MgCl_2$, and Fru-1,6-P_2 at varying concentrations according to the mutant enzyme assay; 50 mM Hepes (pH 8.0); 1.5 units/ml pyrophosphatase; and 0.2 mg/ml bovine serum albumin plus enzyme in a total volume of 0.20 ml. One unit of enzyme activity is 1 μmol of product (either [^{32}P]ATP or ADP-[^{14}C]Glc) formed per min at 37 °C.

Kinetic Characterization

Kinetic data were plotted as specific activity (units/mg) *versus* substrate or effector concentration. Kinetic constants were acquired by fitting the data to the Hill equation with a nonlinear least-square formula using Origin™ Version 5.0. Hill plots were used to calculate the Hill coefficient and the kinetic constants corresponding to the substrate or activator concentrations giving 50% of the maximal velocity ($S_{0.5}$) or activation ($A_{0.5}$).

Thermal Stability

Enzyme samples were in buffer A supplemented with bovine serum albumin to 1 mg/ml in a final volume of 100 μl. Half of the sample (50 μl) was incubated in a water bath equilibrated at 60 °C for 5 min and placed on ice immediately after. The remaining half (50 μl) was kept on ice as a control. The enzyme activities for both the heat-treated and control samples were determined in the ADP-Glc synthesis direction as described for Assay B.

RESULTS

Homology Modeling—We obtained a three-dimensional model of *E. coli* ADP-Glc PPase by comparative modeling using the coordinates of the recently solved crystal structure of the potato tuber ADP-Glc PPase small subunit (Protein Data Bank code 1YP2) as a template as described under "Experimental Procedures" (Fig. 1*A*). Although modeling is generally guaranteed to be successful if residue identity is >40%, for lower percentages, errors can be reduced employing an accurate sequence alignment (43–45). Our two enzymes shared only 33% residue identity; therefore, the alignment was manually edited, incorporating information such as conservation of functional residues and prediction of secondary structures.

Using MODELLER6 Version 1, we generated 143 models after several iterative refinements of the alignment to accommodate gaps, deletions, and insertions of the query sequence with respect to the template in the best possible way. We assessed the models with the program VERIFY_3D (23, 24) as described under "Experimental Procedures," which evaluates the compatibility of a given residue (1D) in a certain environment (3D). A score below zero for a given residue means that the conformation adopted by that residue in the model is not compatible with its surrounding environment. In our study, we considered only those models with all 1D–3D averaged scores above zero; and among them, we chose the one with a profile most similar to that generated by the template crystal structure (Fig. 1*B*). The two profiles followed the same general trend except for two specific regions, both corresponding to residues located in or adjacent to loops not present in the template structure (indicated by *arrows* in Fig. 1*A*). The first, encompassing Phe^{90}–Glu^{97} in the *E. coli* enzyme, aligns with a region in the potato tuber enzyme that is disordered in the crystal structure. The second loop, containing Lys^{259}–Pro^{271}, is an insertion in the bacterial enzyme. Therefore, the final conformation of these two loops in the model, which might also affect immediately adjacent secondary structures, accounted for the differences from the template structure profile. According to the model, these loops are not part of the active site, and they do not contain important conserved residues.

In agreement with our previous biochemical results (46), the modeled monomer shows a two-domain structural organization (Fig. 1*A*). The N terminus of ~300 residues presents a β-α-β motif arranged in an open twisted β-sheet surrounded by α-helices. It resembles the Rossmann fold, typically present in nucleotide-binding domains (47). Residues important for catalysis, Asp^{142} (40), and for substrate binding, Tyr^{114} for ATP (48) and Lys^{195} for Glc-1-P (16), are located in the active-site pocket in close proximity to the ADP-Glc molecule (Fig. 1*C*), observations that further validate the quality of our model. The C terminus is a separate domain folded as a β-helix and linked to the N terminus by a long loop. The two domains are in intimate interaction through extensive hydrophobic contacts, supporting the requirement of a full-length polypeptide to obtain normal enzyme activity and regulation (46).

Selection of Residues for Analysis—The three-dimensional model complexed with ADP-Glc shows the ligand placed in a

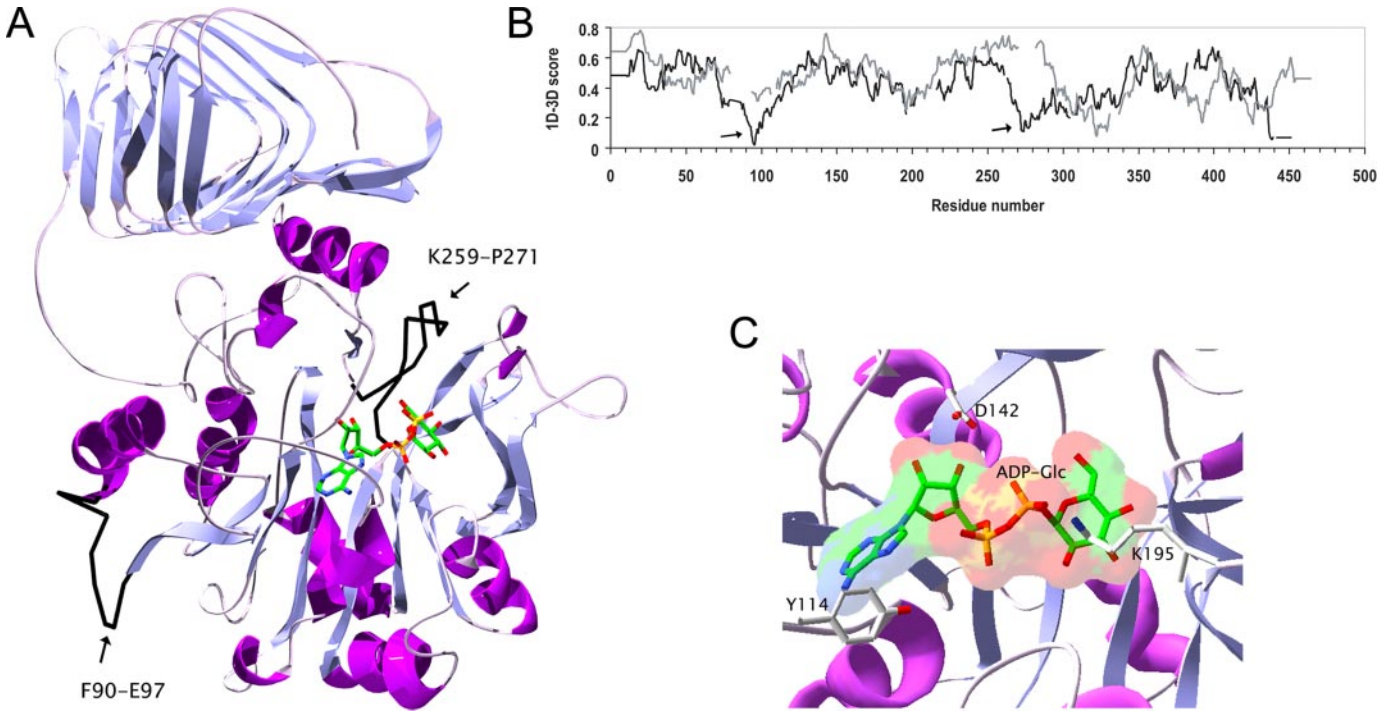

FIGURE 1. **Structural model of *E. coli* ADP-Glc PPase.** *A*, schematic representation of the monomer. The N terminus presents a Rossmann-like fold and holds the ADP-Glc molecule in the active site. Carbons are shown in *green*, and all other atoms are colored by type. The C terminus adopts a β-helix fold and is connected to the N terminus by a long loop. Loops of low structural reliability, comprising Phe^{90}–Glu^{97} and Lys^{259}–Pro^{271}, are shown in *black* and indicated by *arrows*. *B*, Verify_3D profile obtained from assessment of the *E. coli* ADP-Glc PPase structural model. The profile shown in *black* corresponds to our model, and that shown in *gray* corresponds to the template crystal structure. Gaps in the template profile correspond to gaps in the sequence alignment with the *E. coli* enzyme and to stretches of amino acids not solved in the crystal structure. The two big depressions in the *E. coli* profile indicated by *arrows* are regions of low structural reliability and correspond to the Phe^{90}–Glu^{97} and Lys^{259}–Pro^{271} loops. *C*, close-up view of the modeled active site, with a bound ADP-Glc molecule. Carbons are shown in *green*. Asp^{142}, Tyr^{114}, and Lys^{195} (*white* carbons), which are involved in catalysis (40) and in the binding of ATP (48) and Glc-1-P (16), respectively, are in the active site and close to the ligand.

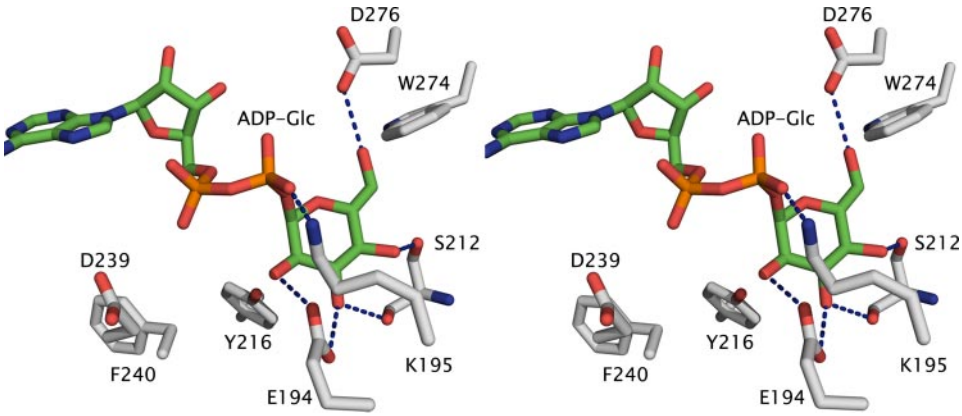

FIGURE 2. ***E. coli* ADP-Glc PPase-substrate interaction.** The stereo representation of the putative Glc-1-P-binding site shows the residues studied in this work (*white* carbons) and their proposed hydrogen bond interactions (*dashed blue lines*) with the bound ADP-Glc molecule (*green* carbons).

well defined pocket in the active site (Fig. 1*A*), and several direct interactions between the ligand and the enzyme are evident (Fig. 2). Lys^{195} makes a salt bridge with the glucose phosphate, an interaction that has been biochemically probed by Hill *et al.* (16) in *E. coli* ADP-Glc PPase and by Fu *et al.* (17) in their analysis of the homologous residue (Lys^{198}) in the potato tuber enzyme. Additionally, the hydroxyl groups of the glucosyl moiety of the ligand are involved in a complex network of hydrogen bonds with the enzyme. The side chains of Glu^{194}, Asp^{276}, and Ser^{212} and the backbone of the latter participate in such interactions.

We performed a multiple sequence alignment using the catalytic subunits of 15 ADP-Glc PPases from several sources, each of them representative of a different taxonomic group. Fig. 3 depicts part of the aligned sequences, comprising residues located in and around the putative Glc-1-P-binding domain in the N terminus of the protein. The residues that, in the model, appear to interact through hydrogen bonds with the glucosyl moiety of the ligand are absolutely conserved among all ADP-Glc PPases analyzed, suggesting that they are involved in a conserved role such as substrate binding. According to our structural model, other conserved residues in this region are also located in the substrate-binding pocket. Based on our observations, we selected Tyr^{216}, Asp^{239}, Phe^{240}, and Trp^{274} to be characterized together with Glu^{194}, Ser^{212}, and Asp^{276}.

Expression and Purification of pMAB3-Single Mutant Plasmids—All selected amino acids were mutated to alanine to analyze their potential role in Glc-1-P interaction. We created additional mutations to investigate whether the observed effect

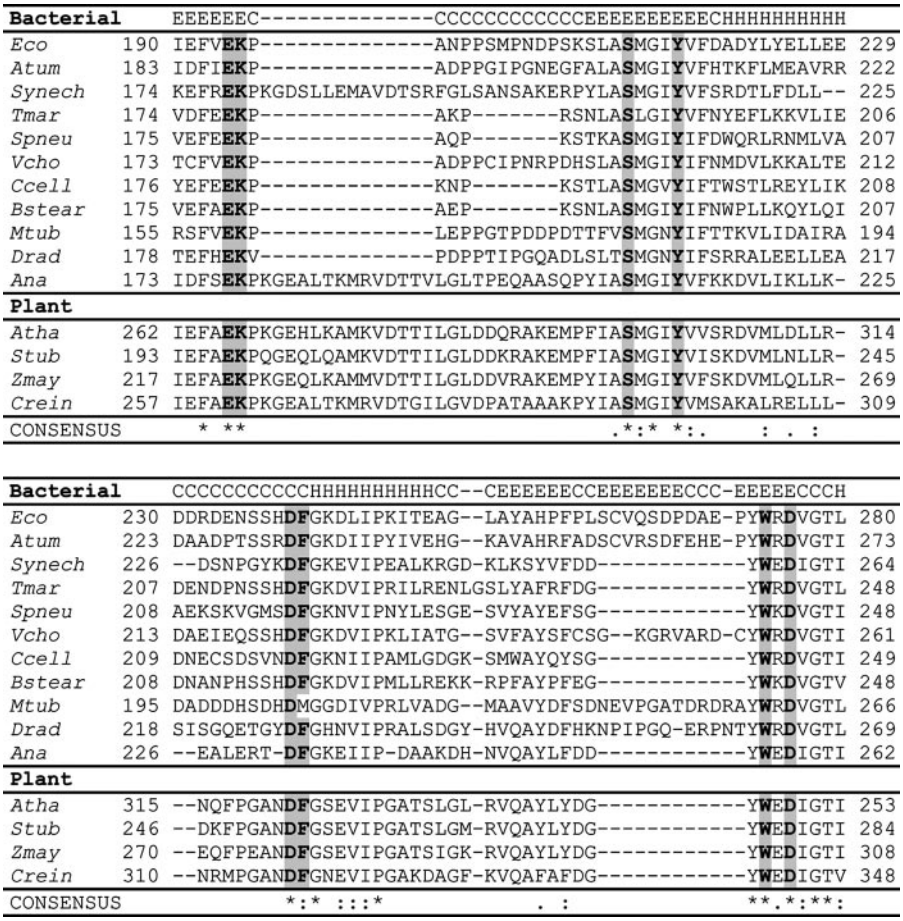

FIGURE 3. **Sequence alignment of *E. coli* ADP-Glc PPase and its homologs.** The primary structures of representative bacterial ADP-Glc PPases and catalytic subunits from photosynthetic organisms were aligned. The region shown here encompasses residues located at and near the putative Glc-1-P-binding site according to our homology model. *Eco*, *E. coli* B; *Atum*, *A. tumefaciens*; *Synech*, *Synechococcus* sp. WH 8102; *Tmar*, *T. maritima*; Spneu, *S. pneumoniae*; *Vcho*, *V. cholerae*; *Ccell*, *C. cellulolyticum*; *Bstear*, *G. stearothermophilus*; *Mtub*, *M. tuberculosis*; *Drad*, *D. radiodurans*; *Ana*, *Anabaena* sp. PCC 7120; *Atha*, *A. thaliana*; *Stub*, *S. tuberosum* (small subunit); *Zmay*, *Z. mays* (small subunit, endosperm); *Crein*, *C. reinhardtii* (small subunit). NCBI accession numbers and references are provided under "Experimental Procedures." The secondary structure prediction is depicted at the top. *E*, β-strand; *C*, coil; *H*, α-helix. The consensus sequence is also shown at the bottom. The residues studied in this work are highlighted in *gray*.

on the affinity for Glc-1-P is due to their shape, size, charge, or aromaticity. *E. coli* wild-type and mutant ADP-Glc PPases were expressed and purified as described under "Experimental Procedures." They had the expected molecular masses upon SDS-PAGE, and they were recognized by the anti-*E. coli* AC70R1 ADP-Glc PPase antibody in immunoblots (data not shown). Y216A either failed to be expressed or rendered the protein completely susceptible to proteolysis because no band ≥10 kDa was detected by immunoblotting in either the soluble or insoluble fractions of the expression cell lysates. After the first chromatographic step, all enzymes were 60–70% pure and suitable for kinetic characterization assays. An additional chromatographic step yielded >95% pure enzymes, which allowed for the proper determination of their specific activities.

Kinetic Characterization—The kinetic characteristics of the mutant enzymes were compared with those of the wild type. All alanine mutations decreased the apparent affinity of the enzyme for the substrate Glc-1-P, as $S_{0.5}$ values for all the mutants were 1 or 2 orders of magnitude larger than that for the wild type (Table 1). The most important increments in this

TABLE 1

Comparison of the specific activities and apparent affinity for the substrate Glc-1-P of the *E. coli* wild-type and mutant enzymes

Determinations were obtained with pure enzymes in the synthesis direction of the reaction by the method of Yep *et al.* (42) as described under "Experimental Procedures."

Enzyme	k_{cat}		Glc-1-P		k_{cat}/K_m
	s^{-1}	-Fold decrease	$S_{0.5}$	-Fold increase	
			μM		$s^{-1}\ mM^{-1}$
Wild-type	370.0 ± 14.4	1.0	17 ± 2	1	21,765
E194A	15.43 ± 0.07	24.0	2812 ± 127	165	6
E194D	92.7 ± 11.7	4.0	6587 ± 1160	388	14
E194Q	80.7 ± 2.0	4.6	1441 ± 369	85	56
S212A	371.2 ± 4.1	1.1	241 ± 34	14	1440
S212V	22.4 ± 1.9	16.5	6416 ± 886	377	4
S212T	179.0 ± 0.7	2.1	4659 ± 274	274	38
S212Y	1.6 ± 0.1	231.2	90 ± 3	5	18
Y216F	29.0 ± 1.0	12.8	785 ± 39	46	37
D239A	32.7 ± 0.2	11.3	524 ± 126	31	62
D239E	347.7 ± 15.9	1.1	169 ± 27	10	2146
D239N	169.0 ± 23.7	2.2	264 ± 38	16	640
F240A	171.7 ± 59.7	2.2	204 ± 10	12	842
F240M	487.0 ± 28.3	0.8	122 ± 4	7	3992
W274A	384.0 ± 23.4	1.0	367 ± 16	22	1046
W274F	266.0 ± 8.0	1.4	50 ± 3	3	5320
W274L	247.5 ± 0.6	1.5	525 ± 32	31	463
D276A	0.36 ± 0.01	1027.8	1706 ± 127	100	0.2
D276N	0.37 ± 0.03	1000.0	1447 ± 151	85	0.3
D276E	112.7 ± 4.5	3.3	416 ± 6	24	275
K195Q[a]	193.3 ± 50	1.9	16,700 ± 380	982	12

[a] Data are from Ref. 16.

kinetic parameter were observed with mutations at Glu^{194} and Ser^{212}. Glc-1-P saturation curves obtained for the Glu^{194} mutants are shown in Fig. 4 as an example to illustrate the shift in the $S_{0.5}$ between the wild type and Glu^{194} mutants. The E194A mutant showed a 165-fold increase (Table 1) compared with the wild type; therefore, we made substitutions to aspartic acid and glutamine to evaluate the importance of the charge and side chain size in such an effect. Mutation to glutamine increased the $S_{0.5}$ for Glc-1-P by 85-fold, pointing out the importance of the negative charge for substrate binding. However, mutation to aspartic acid, which also bears a negative charge, caused a larger negative effect on this kinetic parameter (Table 1), highlighting the significance of the side chain size. These two mutations, E194D and E194Q, caused 4- and 5-fold reduced V_{max} values with respect to the wild type, whereas the E194A mutation decreased the V_{max} by 24-fold. The apparent affinities for ATP, Mg^{2+}, and the activator Fru-1,6-P_2 were not significantly affected by any of these mutations of Glu^{194} (Table 2). Our results validate the hydrogen bonds observed in the structural model (Fig. 2) and strongly suggest that Glu^{194} plays a role in Glc-1-P binding.

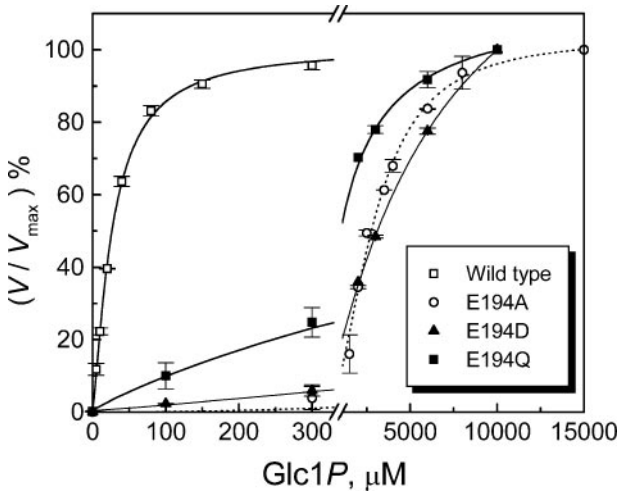

FIGURE 4. **Steady-state kinetic measurement for Glc-1-P dependence for the wild-type and E194A, E194D, and E194Q mutant enzymes.** Initial velocities were determined in the ADP-Glc synthesis direction using Assay B. For wild type (□), E104A (○), E194D (▲), and E104Q (■), V_{max} values were 111.0, 4.6, 27.8, and 24.2 units/mg, respectively. Reactions for each enzyme were performed in the presence of saturating concentrations of ATP, $MgCl_2$, and Fru-1,6-P_2.

Our structural model proposes that Ser^{212} binds O-3 and O-4 of the sugar moiety of the ligand through hydrogen bonds with the side chain and backbone, respectively (Figs. 2 and 6). Here, we probed the role of the side chain in Glc-1-P binding. All Ser^{212} mutations maintained apparent affinity properties for ATP, Mg^{2+}, and Fru-1,6-P_2 at wild-type levels (Table 2). S212A also showed similar k_{cat} values compared with the wild type, but it displayed a 14-fold increased $S_{0.5}$ for Glc-1-P (Table 1). S212V and S212T caused dramatic effects on the apparent affinity for Glc-1-P, with 377- and 274-fold increased $S_{0.5}$ values, respectively (Table 1). Mutation to valine decreased the k_{cat} by ~16-fold, whereas mutation to threonine did so by ~2-fold compared with the wild type. Surprisingly, replacement of Ser^{212} with tyrosine increased the apparent affinity for Glc-1-P by only 5-fold. The k_{cat} for this mutant was, however, 231-fold lower compared with that for the wild type. These results strongly suggest that Ser^{212} is located in the Glc-1-P-binding pocket and that it contributes to the affinity of the enzyme for this substrate.

Asp^{276} was replaced with alanine, asparagine, and glutamic acid. The three mutations decreased the apparent affinity for Glc-1-P by 100-, 85-, and 24-fold, respectively (Table 1). Our results point out the importance of Asp^{276} for Glc-1-P binding and the significance of both the negative charge and size of its side chain on such effect. The analyses of these mutants suggest an additional role for Asp^{276} besides Glc-1-P interaction given that other kinetic parameters were also affected. D276A and D276N had ~1000-fold lower V_{max} values compared with the

TABLE 2

Kinetic parameters of *E. coli* wild-type and mutant ADP-Glc PPases

Reactions were performed in the synthesis direction (Assay B) as described under "Experimental Procedures." Data represent the mean of two or three identical experiments ± the mean difference of the duplicates or triplicates.

Enzyme	ATP		Mg^{2+}		Fru-1,6-P_2	
	$S_{0.5}$	-Fold increase	$S_{0.5}$	-Fold increase	$A_{0.5}$	-Fold increase
	mM		mM		μM	
Wild-type	0.59 ± 0.03	1.0	2.6 ± 0.05	1.0	59.4 ± 4.7	1.0
E194A	1.20 ± 0.04	2.0	7.0 ± 0.6	2.7	321.0 ± 48.1	5.4
E194D	0.49 ± 0.01	0.8	5.3 ± 0.05	2.0	87.0 ± 17.0	1.5
E194Q	0.17 ± 0.08	0.3	4.5 ± 0.2	1.7	20.9 ± 2.8	0.4
S212A	0.68 ± 0.07	1.2	5.1 ± 0.2	2.0	85.3 ± 1.2	1.4
S212V	0.38 ± 0.07	0.7	3.1 ± 0.05	1.2	38.2 ± 4.4	0.6
S212T	0.41 ± 0.04	0.7	3.3 ± 0.2	1.3	37.3 ± 4.2	0.6
S212Y	0.43 ± 0.03	0.7	3.7 ± 0.05	1.4	121.9 ± 11.0	2.0
Y216F	0.35 ± 0.02	0.6	7.8 ± 0.6	3.0	126.0 ± 7.0	2.1
D239A	0.16 ± 0.03	0.3	3.7 ± 0.5	1.4	168.0 ± 9.0	2.8
D239E	0.96 ± 0.03	1.6	5.2 ± 0.1	2.0	118.2 ± 19.6	2.0
D239N	0.56 ± 0.05	0.9	5.6 ± 0.3	2.2	76.6 ± 2.9	1.3
F240A	1.14 ± 0.10	1.9	4.2 ± 0.2	1.6	109.0 ± 40.1	1.8
F240M	1.98 ± 0.14	3.4	5.8 ± 0.3	2.2	72.0 ± 2.1	1.2
W274A	1.04 ± 0.04	1.8	6.0 ± 0.2	2.3	304.0 ± 11.0	5.1
W274F	0.28 ± 0.01	0.5	2.4 ± 0.1	0.9	59.5 ± 9.2	1.0
W274L	0.48 ± 0.03	0.8	3.21 ± 0.01	1.2	226.7 ± 7.0	3.8
D276A	2.03 ± 0.02	3.4	11.2 ± 0.4	4.3	403.0 ± 36.4	7.0
D276N	2.3 ± 0.1	3.9	13.5 ± 2.6	5.2	760.4 ± 49.0	12.8
D276E	4.77 ± 0.04	8.1	15.2 ± 0.2	5.8	281.8 ± 46.8	5.0
K195Q[a]	0.19 ± 0.01	0.3	3.4 ± 0.1	1.3	21 ± 2	0.4

[a] Data are from Ref. 16.

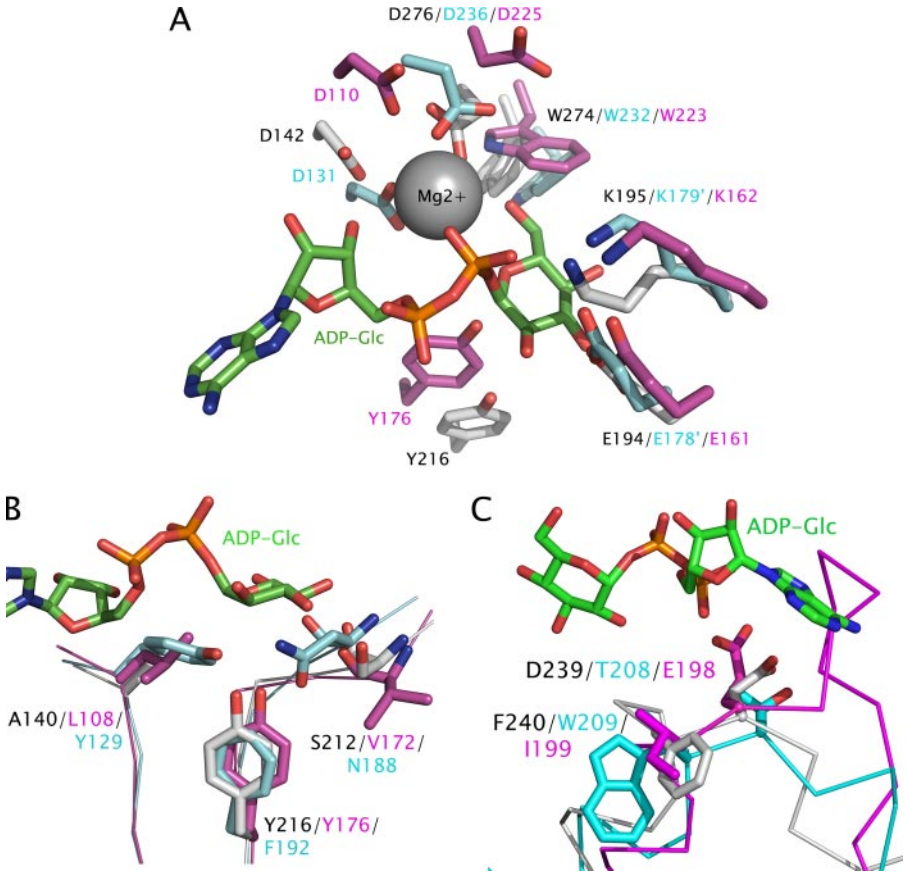

FIGURE 5. **Superposition of the amino acids in the Glc-1-P site from three NDP-Glc PPases.** *A*, superposition of residues from the *E. coli* ADP-Glc PPase model with carbons in *white* (this work) and from the crystal structures of *P. aeruginosa* RmlA (Protein Data Bank code 1G23) with carbons in *magenta* (18) and *S. typhi* CDP-Glc PPase (Protein Data Bank code 1TZF) with carbons in *cyan* (19). The ADP-Glc PPase model has root mean square deviations of 1.9 Å with RmlA and 2.2 Å with CDP-Glc PPase. We show the CDP-Glc PPase active site as it is in the active enzyme, with Asp^{131}, Trp^{232}, and Asp^{236} belonging to one subunit and $Glu^{178'}$ and $Lys^{179'}$ from the neighboring monomer. The ADP-Glc molecule was modeled in ADP-Glc PPase, and Mg^{2+} is present in the CDP-Glc PPase crystal structure. *B*, Ala^{140}, Ser^{212}, and Tyr^{216} in *E. coli* ADP-Glc PPase (*white* carbons) overlaid with the homologous residues Tyr^{129}, Asn^{188}, and Phe^{192} in CDP-Glc PPase (*cyan* carbons) and Leu^{108}, Val^{172}, and Tyr^{176} in RmlA (*magenta* carbons). *C*, Asp^{239} and Phe^{240} in *E. coli* ADP-Glc PPase (*white* carbons) overlaid with the homologous residues Thr^{208} and Trp^{209} in CDP-Glc PPase (*cyan* carbons) and Glu^{198} and Ile^{199} in RmlA (*magenta* carbons).

wild type (Table 1) and 3.4- and ~4-fold higher $S_{0.5}$ values for ATP, respectively (Table 2). D276E displayed a 3-fold decreased V_{max} with respect to the wild type (Table 1) but a bigger change in the apparent affinity for ATP, characterized by an 8-fold increased $S_{0.5}$ for this substrate (Table 2). On the other hand, all three mutations decreased the apparent affinity for Mg^{2+} by ~4–6-fold (Table 2). These results correlate with the role of the Mg^{2+} ion chelator proposed for the homologous residue (Asp^{280}) in the *S. tuberosum* enzyme (14).

Furthermore, the three Asp^{276} mutants had 5–15-fold higher $A_{0.5}$ values for Fru-1,6-P_2 compared with the wild type (Table 2). To investigate whether this residue is involved in the activator site, we studied another mutant. Previous reports showed that deletions of 11 and 15 residues from the N terminus of *E. coli* ADP-Glc PPase render activated enzymes even in the absence of Fru-1,6-P_2, with all other kinetic parameters similar to those of the wild type (39, 49). On the basis of these results, we combined both the N-terminal deletion and the single mutation D276N to create EcNΔ15-D276N. The activity of the partially purified double mutant was 0.027 ± 0.003 units/mg, similar to that of the partially purified D276N single mutant (data not shown), whereas the $A_{0.5}$ for Fru-1,6-P_2 was 51 μM, similar to the that of the wild type (Table 2). This strongly suggests that Asp^{276} is not directly involved in activator binding but is a pivotal residue for the correct interaction of the substrates with the enzyme, influencing the resulting conformational changes upon their binding.

The role of the size and aromaticity of Trp^{274} was studied by substituting it with alanine, leucine, and phenylalanine. Mutation to alanine was characterized by a 22-fold decrease in the apparent affinity for Glc-1-P and did not have significant effect on the V_{max} of the enzyme (Table 1) or on the apparent affinities for ATP, Mg^{2+}, and Fru-1,6-P_2 (Table 2). We obtained similar results when leucine was placed in this position. In contrast, all parameters remained almost unchanged compared with wild-type levels when Trp^{274} was replaced with phenylalanine, indicating that aromaticity is required at this position for proper interaction of Glc-1-P with the enzyme.

Tyr^{216} is conserved not only among ADP-Glc PPases (Fig. 3) but also in RmlA (Tyr^{176}) (Fig. 5, *A* and *B*) (18). Mutation to phenylalanine allowed us to study the role, if any, of the side chain hydroxyl group in this position. The Y216F mutant displayed a 46-fold lower apparent affinity for Glc-1-P (Table 1) and showed small variations in the apparent affinities for ATP, Mg^{2+}, and Fru-1,6-P_2, with 1–3-fold increases in the respective kinetic constants (Table 2). However, this substitution, in which OH was removed, caused a 10-fold decrease in the V_{max} of the mutant enzyme. Our structural model does not show any direct interaction between this residue and bound ADP-Glc (Fig. 2). Our biochemical data suggest, however, that the side chain OH group plays a role in Glc-1-P interaction, possibly by driving the correct positioning of the substrate in the pocket, which also affects the concomitant catalytic reaction.

Asp^{239} and Phe^{240} are also conserved residues that are located in close proximity to the ligand and that do not show any evident interaction with it in the three-dimensional model. However, the D239A mutation decreased the apparent affinity for Glc-1-P by 31-fold and the V_{max} by 11-fold without significant changes in the other kinetic constants. Likewise, D239N and D239E increased the $S_{0.5}$ for Glc-1-P by 16- and 10-fold, respectively, compared with the wild type. In contrast, the V_{max}

TABLE 3

Thermal stability of the wild type and single mutants

Enzyme activity was measured after heat treatment (5 min at 60 °C) or under control conditions (0 °C) as described under "Experimental Procedures."

Enzyme	k_{cat}		Initial activity
	Control	60 °C	
	s^{-1}		%
Wild-type	370.0 ± 14.4	315.8 ± 12.2	85
E194A	15.43 ± 0.07	13.0 ± 1.3	84
E194D	92.7 ± 11.7	75.0 ± 2.3	81
E194Q	80.7 ± 2.0	66.3 ± 6.3	82
S212A	371.2 ± 4.1	335.7 ± 25.9	90
S212V	22.4 ± 1.9	18.0 ± 1.4	81
S212T	179.0 ± 0.7	107.0 ± 11.3	60
S212Y	1.6 ± 0.1	1.1 ± 0.1	70
Y216F	29.0 ± 1.0	24.7 ± 1.3	85
D239A	32.7 ± 0.2	0.5 ± 0.2	2
D239E	347.7 ± 15.9	304.3 ± 20.4	84
D239N[a]	152.0 ± 11.7	90.3 ± 2.7	59
F240A	111.6 ± 2.3	56.7 ± 9.0	51
F240M[a]	254.4 ± 13.4	207.0 ± 3.7	86
W274A	384.0 ± 23.4	<0.02	<0.04
W274F	266.0 ± 8.0	133.1 ± 5.2	50
W274L	247.5 ± 0.6	<0.003	0.6
D276A	0.36 ± 0.01	0.307 ± 0.003	85
D276N	0.37 ± 0.03	0.30 ± 0.03	82
D276E	112.7 ± 4.5	89.4 ± 0.5	79

[a] Enzymes were ~70–80% pure.

of the D239N mutant was 2-fold lower compared with that of the wild type and was not affected by the D239E substitution (Tables 1 and 2). Replacement of Phe^{240} with alanine and methionine affected the apparent affinity for Glc-1-P, with $S_{0.5}$ values 12- and 7-fold higher, respectively, compared with the wild type. No significant changes in the V_{max} and all other kinetic parameters analyzed here were observed with F240A and F240M (Tables 1 and 2). Together, these results suggest that Asp^{239} and Phe^{240} are important residues for Glc-1-P interaction. They also point out the significance of the Asp^{239} negatively charged side chain for proper catalytic activity.

Thermal Stability—The enzymes were also studied with respect to their thermal stability as described under "Experimental Procedures." The wild-type enzyme and all Glu^{194}, Tyr^{216}, and Asp^{276} mutants, as well as S212A, S212V, F240M, and D239E, showed ~80–85% activity after heat treatment (Table 3).

It is interesting to note that mutation of Phe^{240} to alanine caused the thermal stability of the protein to decrease by 50% under the assayed conditions. This result suggests that, at position 240 of *E. coli* ADP-Glc PPase, not only the hydrophobicity but also the size of the side chain is important for the enzyme to adopt proper and heat-stable folding. A similar situation was observed with Trp^{274}. Replacement of this residue with alanine and leucine, two hydrophobic but small side chain amino acids, rendered enzymes with <1% residual activity after heat treatment, whereas phenylalanine in that position allowed the mutant enzyme to retain at least 50% of the activity (Table 3).

Mutants S212T and S212Y retained 60 and 70% of their initial activities, respectively. These mutations affected not only the apparent affinity for Glc-1-P but also the k_{cat}, suggesting a structural distortion of the active site. It is possible that these side chains also misplace significant structural determinants or disrupt important stabilizing interactions in the protein. Mutations of Asp^{239} rendered enzymes with 2, 59, and 84% residual activities after heat treatment when replaced with alanine, asparagine, and glutamic acid, respectively. A negative charge at position 239 is necessary to guarantee the stability of the enzyme at temperatures higher than the optimum for activity.

DISCUSSION

In this work, we have reported the first detailed characterization of the sugar phosphate site and the three-dimensional structure of *E. coli* ADP-Glc PPase, the Glc-1-P site. We selected a set of residues implicated in shaping this substrate pocket by examination of the primary sequences of several ADP-Glc PPases and the three-dimensional structural of the *E. coli* enzyme complexed with ADP-Glc obtained by homology modeling. The role of the selected residues in binding Glc-1-P was probed by site-directed mutagenesis and steady-state kinetics. The kinetic characterization of the individual mutants revealed the importance of the replaced amino acids.

Knowledge of the three-dimensional structure of *E. coli* ADP-Glc PPase is essential to understand the complex network of interactions established between the protein and the substrate for proper binding. The first published ADP-Glc PPase crystal structure is that of the homotetrameric potato tuber small subunit solved by Jin *et al.* (14), which we used as a template to build a model of the *E. coli* enzyme. The sequence identity between these two proteins is 33%, which is close to the lowest range of accepted homology for performing modeling (45). However, the functional similarity between our query and template proteins and a careful inspection of the sequence alignment, which included information on predicted secondary structures and functional conserved residues, increased the probabilities of obtaining a reliable model.

E. coli ADP-Glc PPase has been the subject of numerous structure-function relationship studies, including those aimed to elucidate the functional role of individual amino acids. Previously, Lys^{195} was studied (16) and showed a very specific effect on Glc-1-P interaction. The reported mutations of this residue increased by 100–10,000-fold the $S_{0.5}$ for Glc-1-P without affecting other kinetic constants. To illustrate this, data reported for mutant K195Q have been included here in Tables 1 and 2. These results are consistent with a very specific role of Lys^{195} in the binding of Glc-1-P, probably by ionic interaction between the positively charged side chain ϵ-amino group and the negative phosphate group of Glc-1-P (16, 17). It is possible that the rest of the amino acids in the substrate pocket, which are the subject of this work, interact with the sugar hydroxyls to increase the affinity of the binding and to provide the correct positioning of the ligand for catalysis.

The three-dimensional model of ADP-Glc PPase that we obtained here allowed us to visualize the spatial arrangement of a set of conserved residues potentially involved in the interaction between the enzyme and the substrate Glc-1-P. It has been reported that, although proteins can bind carbohydrates in many different ways, certain amino acids show high propensity to be in a sugar-binding site (50, 51). Some examples are aromatic rings that can pack against the hydrophobic face of a sugar (52) and carboxylates that can form bidentate hydrogen bonds with two adjacent hydroxyls of a saccharide (50). In our model, we identified Trp^{274}, Tyr^{216}, and Phe^{240}, as well as

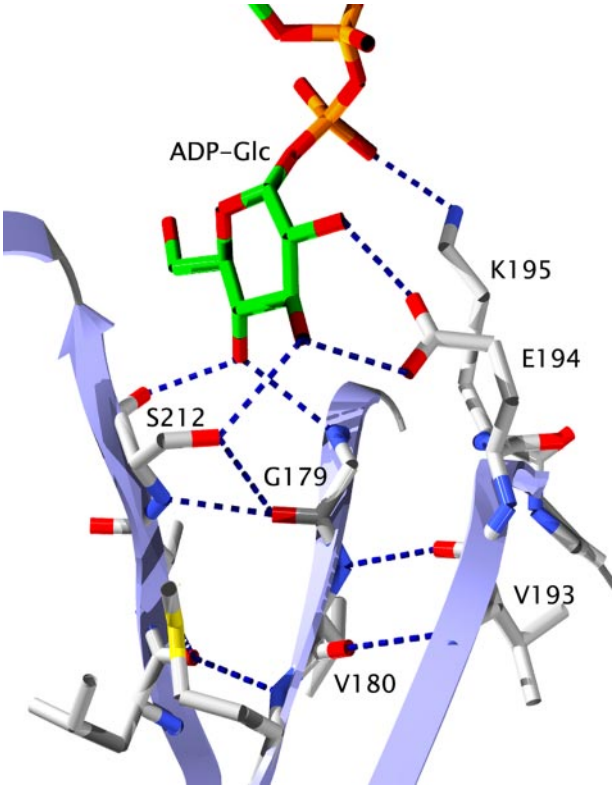

FIGURE 6. **Hydrogen bond network involving Ser^{212} in the *E. coli* ADP-Glc PPase Glc-1-P site.** Ser^{212} interacts with adjacent secondary structures through a complex network of hydrogen bonds (*dashed lines*) involving its side chain and backbone. This network of interactions might be important for the correct positioning of other key residues for Glc-1-P binding, such as Glu^{194} and Lys^{195}.

Glu^{194}, Asp^{239}, and Asp^{276}, some of which show direct contacts with the modeled ligand ADP-Glc.

We also performed a close examination of the reported three-dimensional structures of enzymes that catalyze reactions very similar to those catalyzed by ADP-Glc PPase. These enzymes are *P. aeruginosa* RmlA (Protein Data Bank code 1G23) (18) and *S. typhi* CDP-Glc PPase (Protein Data Bank code 1TZF) (19). We inspected closely their active sites and identified residues homologous to Glu^{194}, Lys^{195}, Asp^{276}, and Trp^{274}, as well as the catalytic Asp^{142} (40), of ADP-Glc PPase in their active sites (Fig. 5*A*). Interestingly, CDP-Glc PPase is a trimeric enzyme with three active sites formed in the interface of adjacent monomers (19). Most of the residues contributing to the architecture of the Glc-1-P site belong to one of the subunits, except for Glu^{178} and Lys^{179}, homologous to Glu^{194} and Lys^{195} in *E. coli* ADP-Glc PPase, which are provided by the neighboring subunit (19).

The ADP-Glc PPase structural model shows the hexose moiety of ADP-Glc largely engaged in hydrogen bonds to surrounding residues (side chains of Lys^{195}, Glu^{194}, Ser^{212}, and Asp^{276}) (Fig. 2) and the protein backbone (Ser^{212} and Gly^{179}) (Fig. 6). Lys^{195} interacts with the β-phosphate of the ADP-Glc molecule. This observation is validated by the biochemical characterization reported by Hill *et al.* (16) and discussed above.

Glu^{194} is proposed to interact with O-2 and O-3 of the sugar ring by a bidentate hydrogen bond. The Glu^{194} mutants displayed the greatest changes in Glc-1-P apparent affinity when substituted with other residues (Table 1). Removal of the negative charge, as observed with the glutamine mutant, caused a large decrease in this kinetic parameter (85-fold), suggesting its importance for substrate interaction. Still, the size of the side chain is also essential given that substitution with aspartic acid decreased the apparent affinity for Glc-1-P by >380-fold. Given that the distance between two atoms engaged in a hydrogen bond is crucial for the establishment of such an interaction, the effect observed with a shorter side chain at position 194 supports the existence of a hydrogen bond between the ligand and Glu^{194}. In addition, the enzyme activity seems to be affected by modifications at this position. It is possible that Glu^{194} plays a key role in positioning the substrate in the correct orientation for catalysis, which also agrees with a critical contribution of size to the functionality of this residue. Our results support the central role of Glu^{194} in Glc-1-P binding and explain the absolute conservation of this amino acid in the ADP-Glc PPase family (Fig. 3) and other NDP-Glc PPases such as RmlA and CDP-Glc PPase (Fig. 5*A*).

Ser^{212} may bind Glc-1-P through hydrogen bonds between the side chain and backbone and O-3 and O-4 of the sugar ring, respectively (Figs. 2 and 6). We probed the role of the side chain OH group in this interaction by making conservative and nonconservative mutations. Although to various degrees, all Ser^{212} mutants affected the apparent affinity for Glc-1-P. Homology modeling of the Ser^{212} mutant active-site residues complexed with ADP-Glc showed that the interaction predicted in the wild-type enzyme model between the Lys^{195} ϵ-amino group and the phosphate of the ligand is disrupted when Ser^{212} is replaced with other amino acid (supplemental Fig. 1). The 14-fold increase in the $S_{0.5}$ for Glc-1-P caused by the S212A mutant might be explained by the disruption of one hydrogen bond between the side chain and O-3 of the glucose moiety of the ligand. Surprisingly, the effect of the side chain OH group provided by threonine is counteracted by the presence of an additional methyl group in comparison with serine. A similar situation is observed with valine in position 212. This extra methyl group largely disrupts the proper conformation of the binding pocket. The model predicts that Ser^{212} is spatially close to secondary structures containing Glu^{194} and Lys^{195} which, as indicated previously, are important in Glc-1-P interaction. Ser^{212} is also largely engaged in a hydrogen bond network with these structures (Fig. 6). These observations might explain how some of the mutations of Ser^{212} affected the apparent affinity for Glc-1-P, as mutations of Glu^{194} and Lys^{195} did. Surprisingly, substitution of Ser^{212} with a bulky side chain amino acid, tyrosine, caused a slight change in the apparent affinity for this substrate specifically. It is possible that, as the homology model predicts, the preferred rotamer for a tyrosine in this position is one directing the phenyl group away from the Glc-1-P pocket, burying the side chain against other hydrophobic side chains and stabilizing this position by a hydrogen bond between the phenyl OH group and an adjacent backbone (data not shown). It is possible that the burying of the phenyl group causes structural arrangements, which probably extend to other parts of the active site, affecting specifically an important catalytic residue. This would be explained by the dramatic reduction in the k_{cat}

displayed by mutant S212Y. Therefore, the side chain of Ser^{212} might contribute to the overall affinity for Glc-1-P by making direct interactions with O-3 of the sugar ring and with adjacent backbones containing important residues for the positioning of this substrate. On the other hand, the model shows the Ser^{212} peptide carbonyl group binding O-4 of the hexose through a hydrogen bond (Figs. 2 and 6). This interaction can also be observed in the crystal structures of the NDP-Glc PPases RmlA (18) and CDP-Glc PPase (19). The peptide carbonyl groups of Val^{172} in RmlA and Asn^{188} in CDP-Glc PPase, homologous to Ser^{212} in ADP-Glc PPase (Fig. 6), also make hydrogen bonds with the substrate, implying that this interaction is important for the correct geometry of Glc-1-P in the binding pocket. Apart from the specific interactions, the size of the side chain is important for the proper architecture of the Glc-1-P-binding site.

Asp^{276} is important for the enzyme interaction with Glc-1-P, and it may bind O-6 of the hexose through a hydrogen bond (Fig. 2). Substitutions with other residues affected the apparent affinity for this substrate by ~25–100-fold, supporting this hypothesis. However, Asp^{276} might have a broader role rather than exclusively interacting with the Glc-1-P molecule because the V_{max} and the apparent affinity for the other substrates were also affected by the mutations studied (Tables 1 and 2). Asp^{276} is spatially close to the catalytic Asp^{142} (40), and its homologous residue in potato tuber ADP-Glc PPase (Asp^{280}) has been proposed as an Mg^{2+} chelator (14). These observations explain why the different substitutions of Asp^{276} also affected other kinetic parameters besides the Glc-1-P apparent affinity. In contrast to the mutations of other residues in the Glc-1-P site, the activation by Fru-1,6-P_2 was also altered in the Asp^{276} mutants (Table 2). The results obtained with EcNΔ15-D276N strongly suggest that this amino acid does not direct participate in activator binding.

Asp^{276} may be located in a hinge-like region of the active site between the ATP and Glc-1-P subdomains. Apart from interacting with the sugar ring and Mg^{2+}, it may also contact other residues from adjacent secondary structures, establishing a network of interactions driving the conformational changes experienced upon binding the substrates. Comparison of the potato tuber ADP-Glc PPase crystal structures complexed with ATP or ADP-Glc illustrates such subdomain movement (14). The observations of Haugen and Preiss (53) also contribute to explaining the negative effects on all the kinetic properties of the enzyme when Asp^{276} was mutated. They demonstrate that (*a*) ATP alone displays half-site occupancy in the homotetrameric enzyme; (*b*) Glc-1-P does not bind to the enzyme unless $MgCl_2$ and ATP are present; and (*c*) ATP displays full-site occupancy in the presence of Glc-1-P. A synergistic effect on the binding of Fru-1,6-P_2 and ATP was also reported. Thus, the cooperative properties and the heterotrophic interactions between substrates and effectors (53) also explain the broad effect on the kinetic properties of the enzyme when the physiochemical properties of this strategically located residue are modified.

Aromatic residues, typically Trp and Phe, are key components of several saccharide-binding sites (52). Usually, these aromatic rings have been found to be involved in stacking interactions against the face of a sugar (50). However, in our structural model, none of the three aromatic residues in close proximity to the glucosyl moiety of the ligand orients its side chain parallel to the sugar ring. The great conservation of Trp^{274} observed among ADP-Glc PPases (Fig. 3) and other pyrophosphorylases (Fig. 5*A*) might be explained by its structural role within the Glc-1-P site. Substitution with short aliphatic side chain amino acids such as alanine and leucine not only affected the apparent affinity for Glc-1-P (Table 1) but also greatly decreased the thermal stability of the enzyme (Table 3). These effects were less when Trp^{274} was mutated to phenylalanine, suggesting that aromaticity is important at this position. This amino acid might provide the necessary stacking interactions to shape the Glc-1-P site correctly while establishing the proper hydrophobic interactions that increase the thermal stability of the protein.

Tyr^{216} is also located close to the ligand, but no evident interaction is observed between the sugar ring and the side chain OH group. We evaluated the role of such a group in Glc-1-P binding with the Y216F mutation, which lower the V_{max} by 10-fold and the apparent affinity for this substrate by 46-fold (Table 1). Tyr^{216} is conserved in all ADP-Glc PPases studied so far (Fig. 3) and is present in RmlA (Tyr^{176}) (Fig. 5, *A* and *B*). In contrast CDP-Glc PPase bears a phenylalanine (Phe^{192}) in the homologous position, but Tyr^{129}, located in an adjacent β-strand, orients its side chain so that the OH group overlaps with those of Tyr^{216} in ADP-Glc PPase and of Tyr^{176} in RmlA (Fig. 5*B*). Given the conservation of the aromatic ring at this position, it is possible that Tyr^{216} plays a structural role in the Glc-1-P site architecture. On the other hand, the OH group could also make a hydrogen bond with a water molecule in direct contact with the substrate, as observed with Tyr^{176} in RmlA (18). This interaction might be crucial to drive the correct positioning of the Glc-1-P molecule for the enzymatic reaction because not only the apparent affinity for this substrate but also the catalytic activity was affected by the removal of the side chain OH group.

We also analyzed the possible roles of Asp^{239} and Phe^{240} as part of the Glc-1-P site. Our results with mutant D239E showed that the change in size significantly affected the apparent affinity for Glc-1-P and that a negative charge at position 239 is necessary to maintain significant enzyme activity and thermal stability (Tables 1 and 3). On the other hand, substitutions with asparagine and alanine caused the greatest alteration in apparent affinity for Glc-1-P, catalytic activity (Table 1), and thermal stability (Table 3). The structures of RmlA and CDP-Glc PPase show other hydrogen bond donors in the position homologous to Asp^{239}: Glu^{198} and Thr^{208}, respectively (Fig. 5*C*). Moreover, in the RmlA structure, Glu^{198} interacts with O-2 of the dTDP-Glc molecule through a bridging water molecule. Hydrogen bonds and ion pairs with ordered water molecules are considered important interactions that increase the thermal stability of the protein (54) and the binding affinity and specificity for the substrate (50). We cannot rule out the possibility that Asp^{239} also interacts with the solvent, which is critical for the correct positioning of Glc-1-P and may also affect the enzyme activity.

The data obtained with Phe^{240} mutants demonstrate that a hydrophobic bulky residue is needed to maintain the properties

of the enzyme at wild-type levels. The role of Phe^{240} might be merely structural, and the effects on Glc-1-P apparent affinity may be a consequence of the close proximity to Asp^{239}. In the three-dimensional model, Phe^{240} is surrounded by a hydrophobic environment, and it is probably necessary to anchor the loop containing Asp^{239} in the correct position. Phe^{240} is conserved in most of the ADP-Glc PPases (Fig. 3), except in those from the *Mycobacterium* sp. taxonomic group, which bear methionine in the homologous position. Similarly, CDP-Glc PPase has Trp^{209}, whereas RmlA has a smaller hydrophobic residue (Ile^{199}) (Fig. 5*C*). Together with our biochemical results, these observations support the role of Phe^{240} as an important structural component of the Glc-1-P site.

In this work, we have presented data supporting that key amino acids in ADP-Glc PPase have a role in the affinity of the enzyme for Glc-1-P. Whether establishing direct hydrogen bonds with the hydroxyls in the sugar ring or solvent molecules or properly shaping the substrate pocket, they all have an important role in determining the architecture of the Glc-1-P site. This is the first thorough biochemical characterization performed on ADP-Glc PPases. We combined biochemical data with information from the three-dimensional model, which allowed us to hypothesize the structural basis of substrate binding. Comparison of our model with other NDP-Glc PPases reveals remarkable similarities, suggesting that the architecture of the Glc-1-P site is conserved. Biochemical data involving the amino acids examined have not been reported on other PPases to date. We believe that the results reported in this work can be extended to other members of the NDP-Glc PPase family, providing new insights toward the understanding of the evolution of these enzymes.

Acknowledgments—We thank Drs. A. Yep and A. A. Iglesias for stimulating discussions and critical review of the manuscript.

REFERENCES

1. Preiss, J. (1984) *Annu. Rev. Microbiol.* **38,** 419–458
2. Iglesias, A. A., and Preiss, J. (1992) *Biochem. Educ.* **20,** 196–203
3. Ghosh, H. P., and Preiss, J. (1966) *J. Biol. Chem.* **241,** 4491–4504
4. Preiss, J., and Sivak, M. N. (1998) in *Comprehensive Natural Products Chemistry: Starch and Glycogen Biosynthesis* (Pinto, B. M., ed) Vol. 3, pp. 441–495, Pergamon Press, Oxford
5. Ballicora, M. A., Iglesias, A. A., and Preiss, J. (2003) *Microbiol. Mol. Biol. Rev.* **67,** 213–225
6. Ballicora, M. A., Iglesias, A. A., and Preiss, J. (2004) *Photosynth. Res.* **79,** 1–24
7. Takata, H., Takaha, T., Okada, S., Takagi, M., and Imanaka, T. (1997) *J. Bacteriol.* **179,** 4689–4698
8. Preiss, J., and Romeo, T. (1994) *Prog. Nucleic Acid Res. Mol. Biol.* **47,** 299–329
9. Sivak, M. N., and Preiss, J. (1998) in *Advances in Food and Nutrition Research* (Taylor, S. L., ed) Vol. 41, pp. 47–49, Academic Press, Inc., San Diego, CA
10. Nakata, P. A., Greene, T. W., Anderson, J. M., Smith-White, B. J., Okita, T. W., and Preiss, J. (1991) *Plant Mol. Biol.* **17,** 1089–1093
11. Smith-White, B. J., and Preiss, J. (1992) *J. Mol. Evol.* **34,** 449–464
12. Ballicora, M. A., Dubay, J. R., Devillers, C. H., and Preiss, J. (2005) *J. Biol. Chem.* **280,** 10189–10195
13. Iglesias, A. A., Kakefuda, G., and Preiss, J. (1991) *Plant Physiol.* **97,** 1187–1195
14. Jin, X., Ballicora, M. A., Preiss, J., and Geiger, J. H. (2005) *EMBO J.* 694–704
15. Lee, Y. M., and Preiss, J. (1986) *J. Biol. Chem.* **261,** 1058–1064
16. Hill, M. A., Kaufmann, K., Otero, J., and Preiss, J. (1991) *J. Biol. Chem.* **266,** 12455–12460
17. Fu, Y., Ballicora, M. A., and Preiss, J. (1998) *Plant Physiol.* **117,** 989–996
18. Blankenfeldt, W., Asuncion, M., Lam, J. S., and Naismith, J. H. (2000) *EMBO J.* **19,** 6652–6663
19. Koropatkin, N. M., and Holden, H. M. (2004) *J. Biol. Chem.* **279,** 44023–44029
20. Fiser, A., Do, R. K., and Sali, A. (2000) *Protein Sci.* 1753–1773
21. Marti-Renom, M. A., Stuart, A., Fiser, A., Sánchez, R., Melo, F., and Sali, A. (2000) *Annu. Rev. Biophys. Biomol. Struct.* 291–325
22. Sali, A., and Blundell, T. L. (1993) *J. Mol. Biol.* **234,** 779–815
23. Luthy, R., Bowie, J., and Eisenberg, D. (1992) *Nature* **356,** 83–85
24. Bowie, J., Luthy, R., and Eisenberg, D. (1991) *Science* **253,** 164–170
25. Baecker, P. A., Furlong, C. E., and Preiss, J. (1983) *J. Biol. Chem.* **258,** 5084–5088
26. Uttaro, A. D., and Ugalde, R. A. (1994) *Gene* (*Amst.*) **150,** 117–122
27. Palenik, B., Brahamsha, B., Larimer, F. W., Land, M., Hauser, L., Chain, P., Lamerdin, J., Regala, W., Allen, E. E., McCarren, J., Paulsen, I., Dufresne, A., Partensky, F., Webb, E. A., and Waterbury, J. (2003) *Nature* **424,** 1037–1042
28. Nelson, K. E., Clayton, R. A., Gill, S. R., Gwinn, M. L., Dodson, R. J., Haft, D. H., Hickey, E. K., Peterson, J. D., Nelson, W. C., Ketchum, K. A., McDonald, L., Utterback, T. R., Malek, J. A., Linher, K. D., Garrett, M. M., Stewart, A. M., Cotton, M. D., Pratt, M. S., Phillips, C. A., Richardson, D., Heidelberg, J., Sutton, G. G., Fleischmann, R. D., Eisen, J. A., White, O., Salzberg, S. L., Smith, H. O., Venter, J. C., and Fraser, C. M. (1999) *Nature* **399,** 323–329
29. Tettelin, H., Nelson, K. E., Paulsen, I. T., Eisen, J. A., Read, T. D., Peterson, S., Heidelberg, J., DeBoy, R. T., Haft, D. H., Dodson, R. J., Durkin, A. S., Gwinn, M., Kolonay, J. F., Nelson, W. C., Peterson, J. D., Umayam, L. A., White, O., Salzberg, S. L., Lewis, M. R., Radune, D., Holtzapple, E., Khouri, H., Wolf, A. M., Utterback, T. R., Hansen, C. L., McDonald, L. A., Feldblyum, T. V., Angiuoli, S., Dickinson, T., Hickey, E. K., Holt, I. E., Loftus, B. J., Yang, F., Smith, H. O., Venter, J. C., Dougherty, B. A., Morrison, D. A., Hollingshead, S. K., and Fraser, C. M. (2001) *Science* **293,** 498–506
30. Heidelberg, J. F., Eisen, J. A., Nelson, W. C., Clayton, R. A., Gwinn, M. L., Dodson, R. J., Haft, D. H., Hickey, E. K., Peterson, J. D., Umayam, L., Gill, S. R., Nelson, K. E., Read, T. D., Tettelin, H., Richardson, D., Ermolaeva, M. D., Vamathevan, J., Bass, S., Qin, H., Dragoi, I., Sellers, P., McDonald, L., Utterback, T., Fleishmann, R. D., Nierman, W. C., White, O., Salzberg, S. L., Smith, H. O., Colwell, R. R., Mekalanos, J. J., Venter, J. C., and Fraser, C. M. (2000) *Nature* **406,** 477–483
31. Fleischmann, R. D., Alland, D., Eisen, J. A., Carpenter, L., White, O., Peterson, J. D., DeBoy, R. T., Dodson, R. J., Gwinn, M. L., Haft, D. H., Hickey, E. K., Kolonay, J. F., Nelson, W. C., Umayam, L. A., Ermolaeva, M. D., Salzberg, S. L., Delcher, A., Utterback, T. R., Weidman, J. F., Khouri, H. M., Gill, J., Mikula, A., Bishai, W., Jacobs, W. R., Jr., Venter, J. C., and Fraser, C. M. (2002) *J. Bacteriol.* **184,** 5479–5490
32. White, O., Eisen, J. A., Heidelberg, J., Hickey, E. K., Peterson, D., Dodson, R. J., Haft, D. H., Gwinn, M., Nelson, W. C., Richardson, D., Moffat, K. S., Qin, H., Jiang, L., Pamphile, W., Crosby, M., Sheng, M., Vamathevan, J., Lam, P., McDonald, L., Utterback, T., Zalewski, C., Makarova, K. S., Aravind, L., Daly, M. J., Minton, K. W., Fleischmann, R. D., Ketchum, K. A., Nelson, K. E., Salzberg, S. L., Smith, H. O., Venter, J. C., and Fraser, C. M. (1999) *Science* **286,** 1571–1577
33. Charng, Y. Y., Kakefuda, G., Iglesias, A. A., Buikema, W. J., and Preiss, J. (1992) *Plant Mol. Biol.* **20,** 37–47
34. Wang, S. M., Lue, W. L., Yu, T. S., Long, J. H., Wang, C. N., Eimert, K., and Chen, J. (1998) *Plant J.* **13,** 63–70
35. Ballicora, M. A., Laughlin, M. J., Fu, Y., Okita, T. W., Barry, G. F., and Preiss, J. (1995) *Plant Physiol.* **109,** 245–251
36. Hannah, L. C., Shaw, J. R., Giroux, M. J., Reyss, A., Prioul, J. L., Bae, J. M., and Lee, J. Y. (2001) *Plant Physiol.* **127,** 173–183
37. Zabawinski, C., Van Den Koornhuyse, N., D'Hulst, C., Schlichting, R., Giersch, C., Delrue, B., Lacroix, J.-M., Preiss, J., and Ball, S. (2001) *J. Bacteriol.* **183,** 1069–1077

38. Ho, S. N., Hunt, H. D., Horton, R. M., Pullen, J. K., and Pease, L. R. (1989) *Gene* (*Amst.*) **15,** 51–59
39. Bejar, C. M., Ballicora, M. A., Iglesias, A. A., and Preiss, J. (2006) *Biochem. Biophys. Res. Commun.* **343,** 216–221
40. Frueauf, J. B., Ballicora, M. A., and Preiss, J. (2001) *J. Biol. Chem.* **276,** 46319–46325
41. Morell, M. K., Bloom, M., Knowles, V., and Preiss, J. (1987) *Plant Physiol.* **85,** 182–187
42. Yep, A., Bejar, C. M., Ballicora, M. A., Dubay, J. R., Iglesias, A. A., and Preiss, J. (2004) *Anal. Biochem.* **324,** 52–59
43. Sánchez, R., and Sali, A. (2000) in *Protein Structure Prediction: Methods and Protocols* (Webster, D. M., ed) Vol. 143, 97–129, Humana Press Inc., Totowa, NJ
44. Sánchez, R., and Sali, A. (1997) *Curr. Opin. Struct. Biol.* **7,** 206–214
45. Tramontano, A. (1998) *Methods* (*San Diego*) **14,** 293–300
46. Bejar, C. M., Ballicora, M. A., Gómez Casati, D. F., Iglesias, A. A., and Preiss, J. (2004) *FEBS Lett.* **573,** 99–104
47. Rossmann, M. G., Liljas, A., Branden, C.-I., and Bansazak, L. J. (1975) in *The Enzymes* (Boyer, P. D., ed) Vol. 11, pp. 61–102, Academic Press, New York
48. Kumar, A., Tanaka, T., Lee, Y. M., and Preiss, J. (1988) *J. Biol. Chem.* **263,** 14634–14639
49. Wu, M. X., and Preiss, J. (2001) *Arch. Biochem. Biophys.* **389,** 159–165
50. Vyas, N. K. (1991) *Curr. Opin. Struct. Biol.* **1,** 732–740
51. Taroni, C., Jones, S., and Thornton, J. M. (2000) *Protein Eng. Des. Sel.* **13,** 89–98
52. Sujatha, M. S., Sasidhar, Y. U., and Balaji, P. V. (2004) *Protein Sci.* **13,** 2502–2514
53. Haugen, T. H., and Preiss, J. (1979) *J. Biol. Chem.* **254,** 127–136
54. Vogt, G., Woell, S., and Argos, P. (1997) *J. Mol. Biol.* **269,** 631–643

Enzyme Catalysis and Regulation:

Molecular Architecture of the Glucose 1-Phosphate Site in ADP-glucose Pyrophosphorylases

Clarisa Maria Bejar, Xiangshu Jin, Miguel Angel Ballicora and Jack Preiss

J. Biol. Chem. 2006, 281:40473-40484.
doi: 10.1074/jbc.M607088200 originally published online November 1, 2006